



Cite this: *Phys. Chem. Chem. Phys.*,
2024, 26, 7602

Exploring the interfacial behavior of ruthenium complexes in ionic liquids: implications for supported ionic liquid phase catalysts†

Daniel Hemmeter,^a Luciano Sanchez Merlinsky,^{bc} Luis M. Baraldo,^{id b}
Florian Maier,^{id a} Federico J. Williams^{id *bc} and Hans-Peter Steinrück^{id *a}

The interaction of metal complexes with ionic liquids, with a particular focus on the stability and surface concentration of the metal centers, is crucial in applications involving catalysts based on supported ionic liquids. In this study, we synthesized the complexes [Ru(tpy)(bpy)Cl][PF₆] and [Ru(tpy)(dcb)Cl][PF₆] (tpy = 2,2',2''-terpyridine, bpy = 2,2'-bipyridine, dcb = 4,4'-dicarboxy-2,2'-bipyridine) and we prepared solutions using the ionic liquids (ILs) 1-ethyl-3-methylimidazolium acetate [C₂C₁Im][OAc] and 1-butyl-3-methylimidazolium hexafluorophosphate [C₄C₁Im][PF₆]. The chemical environment of the Ru(II) metal center and the interfacial behavior of the complexes in the different IL solutions were determined using angle-resolved X-ray photoelectron spectroscopy (ARXPS). In [C₄C₁Im][PF₆], [Ru(tpy)(bpy)Cl][PF₆] maintains its chemical structure, while in [C₂C₁Im][OAc], partial changes in the chemical environment of the Ru center are indicated by XPS, likely due to ligand exchange. The presence of carboxylic acid functional groups in the bipyridyl ligand seems to inhibit this ligand exchange. The investigated complexes do not exhibit surface activity but are depleted from the IL/gas interface. These findings hold significance for the design of new supported ionic liquid phase catalysts based on Ru complexes.

Received 18th January 2024,
Accepted 9th February 2024

DOI: 10.1039/d4cp00247d

rsc.li/pccp

Introduction

Supported ionic liquid phase (SILP) catalysis presents a new and interesting alternative to traditional heterogeneous catalysis.¹ SILP catalysts comprise a thin ionic liquid (IL) film containing a dissolved catalytically active transition metal complex, dispersed across the large inner surface area of a porous solid support.² Consequently, homogeneous catalysis occurs within a liquid environment at the microscopic level, while the catalyst material remains solid on the macroscopic scale. These systems conveniently combine the advantages of homogeneous and heterogeneous catalysts, offering uniform active sites, efficient metal utilization, and easy separation from reactants and products.³

The very high surface areas and small thicknesses of the immobilized IL film make the structure of the gas/IL interface a particularly interesting parameter for the overall performance

in SILP catalysis.⁴ Previous studies have indicated that the nature of the ligands influence the concentration profile of the catalyst complex in solution, which may range from homogeneous distribution to surface enrichment or depletion at the interface.^{5–13} If the catalyst tends to accumulate near the gas/IL interface, the total process is expected to be more efficient. Therefore, it is crucial to determine the factors influencing the surface enrichment of catalysts in ILs, a matter that has not been fully elucidated yet. Another significant factor is the stability of the dissolved metal complex in the IL, as alterations in the chemical environment of the active site are likely to have a decisive impact on catalytic performance. It is well-established that ILs can function as non-innocent solvents, for example, by coordinating with the metal center^{12,14} in a complex or by facilitating nanoparticle formation.¹⁵

The unique properties of the Ru(II) polypyridine complexes, such as their strong light absorption in the visible range, long-lived excited states, and good chemical stability, resulted in their application in various fields, including photochemotherapy,¹⁶ multicomponent devices,¹⁷ dye-sensitized solar-cells,^{18,19} and catalysts for the water oxidation reaction.²⁰ Furthermore, Ru complexes have demonstrated success as catalysts in ILs.^{21–25} More recently, the SILP concept has been employed to immobilize Ru complexes for the conversion of CO₂ into value-added compounds.²⁶ Therefore, it is important to investigate the

^a Lehrstuhl für Physikalische Chemie II, Universität Erlangen-Nürnberg, Egerlandstraße 3, Erlangen, Germany. E-mail: hans-peter.steinrueck@fau.de

^b Departamento de Química Inorgánica, Analítica y Química Física, Facultad de Ciencias Exactas y Naturales, Universidad de Buenos Aires, Buenos Aires, Argentina. E-mail: fwilliams@qi.fcen.uba.ar

^c Instituto de Química Física de los Materiales, Medio Ambiente y Energía, CONICET-Universidad de Buenos Aires, Buenos Aires, Argentina

† Electronic supplementary information (ESI) available. See DOI: <https://doi.org/10.1039/d4cp00247d>

interaction of Ru complexes with ionic liquids with a particular focus on the stability and surface segregation or depletion of the metal centers, as these aspects play a pivotal role in applications.

In this study, we examined the surface structure and stability of polypyridyl ruthenium complexes in imidazolium-based ionic liquids, namely, 1-ethyl-3-methylimidazolium acetate ($[\text{C}_2\text{C}_1\text{Im}][\text{OAc}]$) and 1-butyl-3-methylimidazolium hexafluorophosphate ($[\text{C}_4\text{C}_1\text{Im}][\text{PF}_6]$). To accomplish this, we employed angle-resolved X-ray photoelectron spectroscopy (ARXPS) to investigate the IL/vacuum interface, enabling a quantitative analysis of the chemical composition of the near-surface region.^{4,27} We determined the surface chemical composition of the ILs, surface enrichment effects, and the chemical state of the dissolved metal complexes.

Experimental methods

$[\text{Ru}(\text{tpy})\text{Cl}_3]$, dcb and $[\text{Ru}(\text{tpy})(\text{bpy})\text{Cl}][\text{PF}_6]$ were prepared according to previous reports (tpy = 2,2',2''-terpyridine, bpy = 2,2'-bipyridine, dcb = 4,4'-dicarboxy-2,2'-bipyridine).^{28–30} ILs 1-butyl-3-methylimidazolium hexafluorophosphate ($[\text{C}_4\text{C}_1\text{Im}][\text{PF}_6]$, purity: 99%) and 1-ethyl-3-methylimidazolium acetate ($[\text{C}_2\text{C}_1\text{Im}][\text{OAc}]$, purity: 98%) were purchased from Iolitec and used as delivered. All other materials used for synthesis were of reagent grade and obtained commercially without further purification.

$[\text{Ru}(\text{tpy})(\text{dcb})\text{Cl}][\text{PF}_6]$ was synthesized as follows: 199 mg of $\text{Ru}(\text{tpy})\text{Cl}_3$ (0.45 mmol), 110 mg of 4,4'-dicarboxy-2,2'-bipyridine (0.45 mmol) and 157 mg of LiCl were heated at reflux for 4 h in a 40 mL solution of ethanol–water (75 : 25) and 0.2 mL of triethylamine. The mixture was filtered hot and its volume reduced to 10 mL. After adding 1 mL of HCl (1 M) it was chilled in the refrigerator for 24 h, affording a dark purple/black precipitate over a red solution. The product was filtered and washed with water (3 × 5 mL), acetone (5 mL) and diethyl ether (10 mL) and then dried in a vacuum desiccator for 24 h. The solid was then dissolved in methanol (5 mL) and precipitated with a KPF₆-saturated water solution (3 mL). Finally, the product was filtered and washed with water (5 mL), ethanol (5 mL) and diethyl ether (10 mL). Yield: 270 mg (79%). Anal. calc. for $[\text{Ru}(\text{tpy})(\text{dcb})\text{Cl}][\text{PF}_6] \cdot 3\text{H}_2\text{O}$: C, 39.9; H, 3.1; N, 8.6. Found: C, 40.3; H, 3.0; N, 8.7. ¹H-NMR (500 MHz, DMSO-d₆): δ ppm 10.27 (d, 1H); 9.28 (s, 1H); 8.99 (s, 1H); 8.84 (d, 2H); 8.70 (d, 2H); 8.45 (dd, 1H); 8.29 (t, 1H); 8.01 (t, 2H); 7.62 (d, 3H); 7.45 (dd, 1H); 7.35 (t, 2H).

The mixtures of $[\text{Ru}(\text{tpy})(\text{bpy})\text{Cl}][\text{PF}_6]$ and $[\text{Ru}(\text{tpy})(\text{dcb})\text{Cl}][\text{PF}_6]$ in 1-ethyl-3-methylimidazolium acetate $[\text{C}_2\text{C}_1\text{Im}][\text{OAc}]$ and 1-butyl-3-methylimidazolium hexafluorophosphate $[\text{C}_4\text{C}_1\text{Im}][\text{PF}_6]$ with 2.5%_{mol} nominal concentration were prepared by stirring the complex powder in the ILs under ambient conditions for at least 2 h. $[\text{Ru}(\text{tpy})(\text{bpy})\text{Cl}][\text{PF}_6]$ in $[\text{C}_4\text{C}_1\text{Im}][\text{PF}_6]$ and $[\text{Ru}(\text{tpy})(\text{dcb})\text{Cl}][\text{PF}_6]$ in $[\text{C}_2\text{C}_1\text{Im}][\text{OAc}]$ gave saturated solutions with minor amounts of remaining solid. $[\text{Ru}(\text{tpy})(\text{dcb})\text{Cl}][\text{PF}_6]$ in $[\text{C}_4\text{C}_1\text{Im}][\text{PF}_6]$ yielded a suspension with a more or less undissolved complex, as concluded from visual inspection; in line with

this, the absence of complex-related signals in XPS confirms the very low solubility. $[\text{Ru}(\text{tpy})(\text{bpy})\text{Cl}][\text{PF}_6]$ in $[\text{C}_2\text{C}_1\text{Im}][\text{OAc}]$ gave a clear solution without any visual solid residuals. The exact weighed proportions are given in Table S2 in the (ESI[†]). A drop of the liquid samples was taken from the bulk of the solution and placed onto the setup-compatible molybdenum sample holders.²⁷ In case of the saturated solutions, solid residuals settled to the ground of the sample holder reservoir, and thus were not detected in the surface analysis by XPS. The samples were left for degassing in the fast-entry load lock of the ultra-high vacuum (UHV) system for several hours before conducting further experiments.

The ARXPS measurements were performed using the dual analyzer system for surface analysis (DASSA), which comprises two electron analysers mounted for simultaneous measurements at 0° and 80° emission relative to the surface normal of macroscopically thick non-volatile liquid samples.²⁷ Simultaneous detection at the two angles has the advantages of avoiding sample tilting, minimizing beam damage, and ensuring that the ARXP spectra are measured at the same time under the exact same conditions. ARXPS at $\vartheta = 0^\circ$ (normal emission) probes the near-surface region with an information depth (ID) of 6–9 nm for organic materials, while the ID at $\vartheta = 80^\circ$ decreases to 1–1.5 nm, which mainly corresponds to the top-most surface layer of the sample.²⁷ Measurements were carried out using a monochromatized X-ray source with Al K α radiation (XM 1000, $h\nu = 1486.6$ eV, 238 W). Survey scans were recorded with a pass energy of 150 eV, and region scans with 35 eV (~0.4 eV combined energy resolution). The binding energy scale was referenced to the C 1s signal of carbon atoms solely bound to other carbon atoms and hydrogen ($\text{C}_{\text{alkyl/aryl}}$) at 285.0 eV. 80° spectra were referenced to the binding energy of the N 1s signal originating from nitrogen atoms of the imidazolium ring N_{im} signal at 0°. Quantitative analysis of peak intensities was conducted using atomic sensitivity factors (ASFs).³¹ The XP spectra were normalized to the overall intensity (sum over all ASF-corrected intensities) of the nominal 2.5%_{mol} solution of $[\text{Ru}(\text{tpy})(\text{bpy})\text{Cl}][\text{PF}_6]$ in $[\text{C}_2\text{C}_1\text{Im}][\text{OAc}]$ recorded at 0°. Each set of 80° spectra was scaled up by an individual geometry factor to compensate for lower intensity compared to 0° spectra. After this normalization, intensity differences between 80° and 0° emission angle can be directly translated into enrichment/depletion effects or preferential orientations of ions at the outer surface. Additional fitting procedures of XP spectra are presented in the ESI.[†] In order to remove an unwanted surface-active contamination in the solution of $[\text{Ru}(\text{tpy})(\text{dcb})\text{Cl}][\text{PF}_6]$ in $[\text{C}_2\text{C}_1\text{Im}][\text{OAc}]$ (as discussed below) the sample was mildly sputtered using Ar⁺ ions (1 kV, 10 mA, 30 s).

Results and discussion

The chemical structures of the Ru polypyridyl complexes and the ILs employed are shown in Fig. 1. Solutions of $[\text{Ru}(\text{tpy})(\text{bpy})\text{Cl}][\text{PF}_6]$ and $[\text{Ru}(\text{tpy})(\text{dcb})\text{Cl}][\text{PF}_6]$ in $[\text{C}_2\text{C}_1\text{Im}][\text{OAc}]$ and $[\text{C}_4\text{C}_1\text{Im}][\text{PF}_6]$ with 2.5%_{mol} nominal concentration were prepared and investigated using XPS. In the complexes, the Ru(II) metal center

is hexa-coordinated, terpyridine is a tridentate ligand, bipyridine is a bidentate ligand, and the remaining position is coordinated by a Cl^- ion. The overall charge of the complexes is +1 and the counterion is hexafluorophosphate $[\text{PF}_6]^-$ in both cases. The ILs employed have a similar imidazolium cation, $[\text{C}_2\text{C}_1\text{Im}]^+$ and $[\text{C}_4\text{C}_1\text{Im}]^+$, differing only in the length of one of the side chains. However, they have different anions, namely hexafluorophosphate, the same anion present in the Ru complexes, or acetate. The high basicity of the acetate anion potentially results in deprotonation of the C_2 carbon of the N,N' -disubstituted imidazolium cation producing N-heterocyclic carbenes (NHCs) and acetic acid.^{32–34} Note that NHCs could potentially act as ligands modifying the chemical structure of the complexes.^{35,36} $[\text{C}_2\text{C}_1\text{Im}][\text{OAc}]$ was subject of a recent ARXPS and molecular dynamics (MD) study by the Newberg group addressing the surface structure of a mixture with $[\text{C}_2\text{C}_1\text{Im}][\text{Tf}_2\text{N}]$.³⁷ However, to the best of our knowledge, neat $[\text{C}_2\text{C}_1\text{Im}][\text{OAc}]$ was not characterized using ARXPS before; hence, we provide a detailed description herein.

$[\text{C}_4\text{C}_1\text{Im}][\text{PF}_6]$ and $[\text{C}_2\text{C}_1\text{Im}][\text{OAc}]$

We first address the characterization of the employed neat ILs by ARXPS. A full ARXPS characterization of neat $[\text{C}_4\text{C}_1\text{Im}][\text{PF}_6]$ was previously reported by our group.³⁸ A corresponding set of XP spectra of the commercial $[\text{C}_4\text{C}_1\text{Im}][\text{PF}_6]$ batch used in this study, measured at 0° (black, normal emission) and 80° (red, grazing emission) is shown in Fig. S1 in the (ESI[†]). While 0° emission spectra typically provide information on the bulk composition of the sample, 80° emission spectra mainly reflect the structure of the topmost molecular layer at the surface. The XP spectra, in particular the increase of the alkyl C 1s signals at 80° , and the quantitative analysis shown in Table 1a, confirm

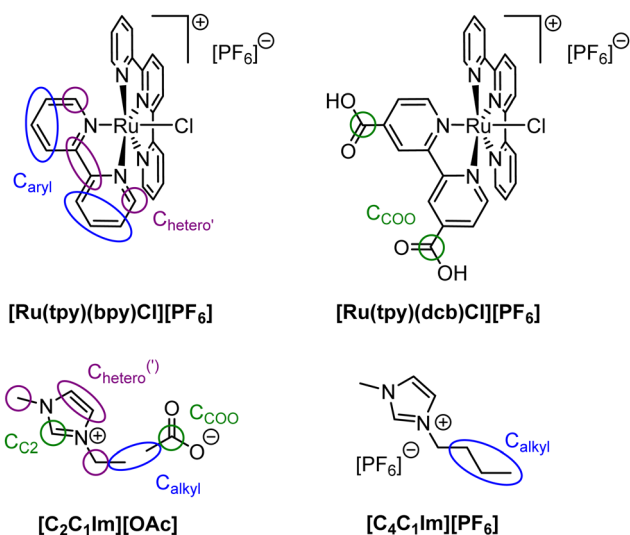


Fig. 1 Chemical structures of the Ru complexes $[\text{Ru}(\text{tpy})(\text{bpy})\text{Cl}][\text{PF}_6]$ and $[\text{Ru}(\text{tpy})(\text{dcb})\text{Cl}][\text{PF}_6]$ and ionic liquids $[\text{C}_2\text{C}_1\text{Im}][\text{OAc}]$ and $[\text{C}_4\text{C}_1\text{Im}][\text{PF}_6]$ employed in this work with assignment of XPS signals to the molecular structure (note that for sake of clarity the assignment of carbon species from the ligands is only shown for bpy. XPS signals from the tpy and dcb ligands were assigned accordingly).

the previously observed interfacial behavior. In brief, the $[\text{C}_4\text{C}_1\text{Im}]^+$ cation of $[\text{C}_4\text{C}_1\text{Im}][\text{PF}_6]$ shows a preferred surface orientation with the alkyl chains terminating the IL/vacuum interface with the cationic headgroups and anions located below.

Fig. 2a shows the C 1s, N 1s and O 1s XP spectra of $[\text{C}_2\text{C}_1\text{Im}][\text{OAc}]$ in normal and grazing emission (note that a wide scan is depicted in Fig. S2 in the ESI[†]). In the C 1s region, several species can be distinguished according to an established deconvolution procedure for the well-studied 1,3-alkylimidazolium ILs.²⁷ The corresponding fit along with the assignment of signals to the molecular structure is shown in Fig. 2b: carbon atoms bound to two heteroatoms, that is, the carbon atom in C_2 position in the imidazolium ring and the carbon atom in the carboxylate group, were detected at 287.4 eV to give a joint signal $\text{C}_{\text{C}_2/\text{COO}}$ (green). Carbon atoms bound to one heteroatom in the imidazolium ring C_{hetero} (violet) and carbon atoms solely bound to other carbon atoms and hydrogen in cation and anion C_{alkyl} (blue) were detected at 286.4 and 285.0 eV, respectively. The N 1s region shows a single peak at 401.8 eV corresponding to the equivalent nitrogen atoms in the cationic heterocycle. The O 1s region shows a major signal at 530.4 eV, which corresponds to the oxygen atoms in the acetate anion. At higher binding energies, the spectrum shows a small broad peak between 532 and 534 eV (marked as * in spectrum; also see inset in O 1s spectrum for $5\times$ enhanced signal), which is more visible in the spectra of the solutions presented below; a similar peak is also visible in spectra reported by Gokturk *et al.*³⁹ This feature could be due to the presence and/or slow, continuous build-up of acetic acid under UHV conditions, which is formed upon deprotonation of $[\text{C}_2\text{C}_1\text{Im}]^+$ cations to produce NHCs.^{32–34} Even though the presence of NHC complexes in $[\text{OAc}]^-$ ILs is still under debate in the literature,³² acetic acid has been detected as an evaporation product of $[\text{C}_2\text{C}_1\text{Im}][\text{OAc}]$ by UPS (gas phase) and mass spectrometry.³⁴ We confirm this finding by quadrupole mass spectrometry, as shown in Fig. S3a (ESI[†]). When studying $[\text{C}_2\text{C}_1\text{Im}][\text{OAc}]$, CH_3COOH -specific signals are found at 12–18 amu, 24–31 amu and 60 amu.⁴⁰ They show minor intensity at room temperature, but strongly increase at 50°C . The quantitative analysis of the 0° and 80° XP spectra is provided in Table 1b. The data is in accordance with literature,³⁹ and the stoichiometry derived from the 0° emission spectra in Fig. 2a shows excellent agreement with the nominal composition of the IL. Comparing 0° and 80° emission spectra in Fig. 2a reveals a minor increase in intensity for the C_{alkyl} signal, while C_{hetero} and N 1s signals slightly decrease. In analogy to the interfacial behavior of the $[\text{C}_4\text{C}_1\text{Im}]^+$ cation mentioned above, this is an indication for a preferred orientation of the $[\text{C}_2\text{C}_1\text{Im}]^+$ cation with the aliphatic moieties directed towards the vacuum. Also, the O 1s signal shows a slight decrease at 80° , which indicates a preferential surface orientation of the $[\text{OAc}]^-$ anion with the methyl group occupying the outer surface, while the charged carboxylate group is pointing towards the bulk. These arrangements are in accordance with results on the organization of ions at the IL/vacuum interface in an IL mixture presented by the Newberg group.³⁷

Table 1 Quantitative analysis of XPS core level spectra of (a) neat $[C_4C_1Im][PF_6]$, (b) neat $[C_2C_1Im][OAc]$ and nominal 2.5%_{molar} solutions of (c) $[Ru(tpy)(bpy)Cl][PF_6]$ in $[C_4C_1Im][PF_6]$, (d) $[Ru(tpy)(bpy)Cl][PF_6]$ in $[C_2C_1Im][OAc]$ and (e) $[Ru(tpy)(dcb)Cl][PF_6]$ in $[C_2C_1Im][OAc]$ (the surface of the latter solution was cleaned by sputtering). Note that the binding energies of spin-orbit-resolved signals correspond to the more intense signal at lower binding energy, that is, Ru $3d_{5/2}$, Cl $2p_{3/2}$ and P $2p_{3/2}$

	Ru 3d	Ru $d_{5/2}$	low BE	Cl 2p	C 1s $C_2/(COO)$	C 1s hetero	C 1s alkyl	N 1s Im	N 1s ligand	O 1s OH	O 1s OAc	F 1s	P 2p
(a) Neat $[C_4C_1Im][PF_6]$													
Binding energy/eV					287.4	286.5	285.0	401.9				686.5	136.6
Nominal					1	4	3	2				6	1
Experimental, 0°					1.0	4.0	2.8	1.9				6.1	1.1
Experimental, 80°					1.0	3.8	3.4	1.8				5.9	1.1
(b) Neat $[C_2C_1Im][OAc]$													
Binding energy/eV					287.4	286.4	285.0	401.8			530.4		
Nominal					2	4	2	2			2		
Experimental, 0°					2.1	4.1	1.8	2.0			2.0		
Experimental, 80°					2.0	4.1	2.0	1.9			2.0		
(c) 2.5%_{molar} $[Ru(tpy)(bpy)Cl][PF_6]$ in $[C_4C_1Im][PF_6]$													
Binding energy/eV	280.8			—	287.4	286.5	285.0	401.9	399.9			686.4	136.4
Nominal	0.025			0.025	1.0	4.3	3.4	2.0	0.13			6.2	1.0
Experimental, 0°	0.013			—	1.0	4.2	3.1	2.0	0.064			6.4	1.2
Experimental, 80°	0.007			—	1.0	4.2	3.9	1.9	0.051			5.8	1.1
(d) 2.5%_{molar} $[Ru(tpy)(bpy)Cl][PF_6]$ in $[C_2C_1Im][OAc]$													
Binding energy/eV	280.9	280.0		198.0	287.5	286.4	285.0	401.7	399.9		530.3	686.5	136.7
Nominal	0.025	0		0.025	2.0	4.3	2.4	2.0	0.13		2.0	0.15	0.025
Experimental, 0°	0.020	0.004		0.026	2.1	4.5	2.2	1.9	0.064		2.0	0.15	0.032
Experimental, 80°	0.009	0.005		—	2.0	4.3	2.8	1.8	0.040		1.9	0.11	0.025
(e) 2.5%_{molar} $[Ru(tpy)(dcb)Cl][PF_6]$ in $[C_2C_1Im][OAc]$ (sputtered)													
Binding energy/eV	280.9			197.7	287.5	286.4	285.0	401.7	399.9	531.4	530.3	686.5	136.7
Nominal	0.026			0.026	2.1	4.3	2.4	2.0	0.13	0.10	2.0	0.15	0.026
Experimental, 0°	0.012			0.015	2.1	4.4	2.0	2.1	0.074	0.089	2.0	0.073	0.004
Experimental, 80°	0.004			—	2.1	4.5	2.3	2.0	0.043	0.17	1.9	0.061	

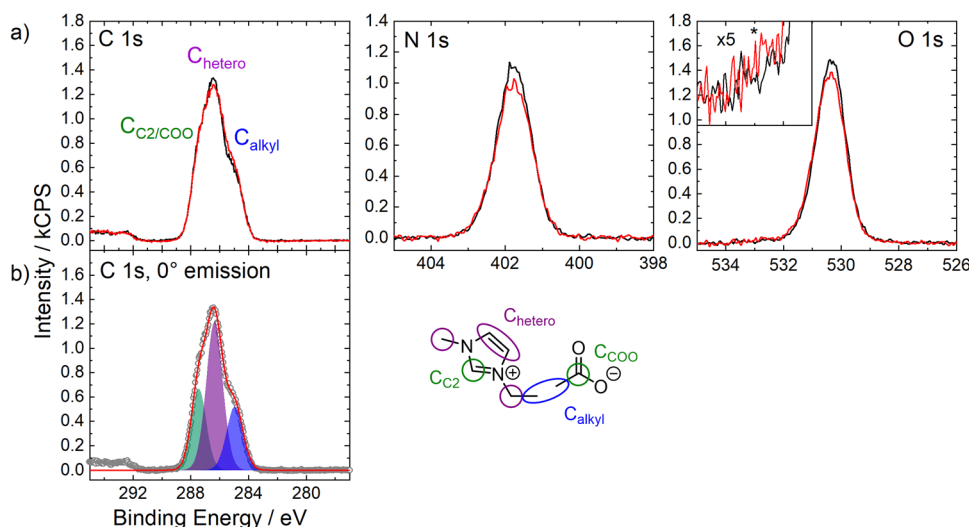


Fig. 2 (a) C 1s (left), N 1s (middle) and O 1s (right) spectra of neat $[C_2C_1Im][OAc]$ in 0° (black) and 80° (red) emission and (b) C 1s spectrum in 0° emission with applied deconvolution and assignment of peaks to the molecular structure. All spectra were recorded at room temperature.

Nominal 2.5%_{molar} solution of $[Ru(tpy)(bpy)Cl][PF_6]$ in $[C_4C_1Im][PF_6]$

Fig. 3a shows the C 1s/Ru 3d, N 1s and F 1s XP spectra corresponding to a nominal 2.5%_{molar} solution of $[Ru(tpy)(bpy)Cl][PF_6]$ in $[C_4C_1Im][PF_6]$; the full set of spectra along with a wide

scan is shown in Fig. S4 in the ESI.† Apart from the signals corresponding to the IL solvent (*cf.* Fig. S1, ESI[†]), the Ru $3d_{5/2}$ peak is observed at 280.8 eV confirming dissolution of the complex. The observed binding energy is in a comparable range reported for a series of Ru(II) complexes in the solid state.⁴¹

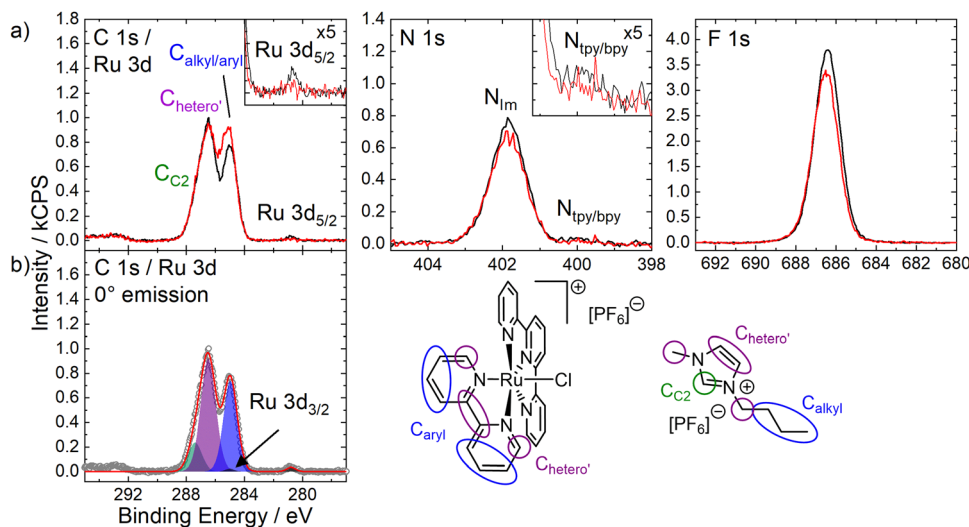


Fig. 3 (a) C 1s/Ru 3d (left), N 1s (middle) and F 1s (right) spectra of a nominal 2.5%_{mol} solution of [Ru(tpy)(bpy)Cl][PF₆] in [C₄C₁Im][PF₆] in 0° (black) and 80° (red) emission and (b) C 1s/Ru 3d spectrum in 0° emission with applied deconvolution and assignment of peaks to the molecular structure (note that for sake of clarity the assignment of carbon species from the ligands is only shown for bpy). XPS signals from the tpy ligand were assigned accordingly. All spectra were recorded at room temperature.

However, it should be noted that interactions of the solute with the IL could result in significant shifting of the metal signal (up to ~ 1.1 eV for Pd 3d_{5/2} in a solution of an *in situ* formed phosphine-imidazolylidene Pd complex in [C₈C₁Im][Tf₂N] compared to a solution of the same complex in [C₈C₁Im][OAc],¹⁴ but oftentimes less pronounced^{42,43}). The Ru 3d_{3/2} signal is hidden underneath the C_{alkyl/aryl} signal with a spin-orbit-induced binding energy difference of 4.2 eV with respect to the Ru 3d_{5/2} signal. The Ru 3d_{3/2} signal was fitted according to the expected intensity ratio of 2:3 for d_{3/2} and d_{5/2} orbitals, as is shown in Fig. 3b. In the N 1s region, in addition to the N_{Im} peak at 401.9 eV, a low intensity peak, N_{tpy/bpy}, is observed at 399.9 eV, which is assigned to the N atoms in the polypyridine ligands.

Table 1c shows the nominal and experimentally determined composition of the nominal 2.5%_{mol} solution of [Ru(tpy)(bpy)-Cl][PF₆] in [C₄C₁Im][PF₆]. The amount of Ru observed is lower than the nominal one, as deduced from the quantitative analysis of the signal in 0° emission, which yields a Ru complex concentration of $\sim 1.3\%$ _{mol} in the IL (notably, the XP signal at 0° stems to ~ 85 – 90% from the IL bulk and only to 10–15% from the topmost surface layer; thus, it is considered a quite accurate estimate for the bulk composition, even in cases where the topmost layer is depleted from a certain species). We thus attribute the too low Ru content in the IL solution to $\sim 50\%$ of undissolved complex, due to a lower solubility of the complex than the nominal 2.5%_{mol} (saturated solution, see Experimental section). Notably, the Ru : N_{tpy/bpy} ratio agrees well with the expected stoichiometry of the complex. This observation suggests that the chemical interaction of the Ru(II) metal center and the tpy and bpy ligands is preserved in the IL solution. However, no Cl 2p signal (expected at ~ 198 eV for Cl 2p_{3/2}) could be unequivocally resolved (see Fig. S4 in the ESI†), due to the low concentration of the complex in [C₄C₁Im][PF₆] and the low cross-section of the Cl 2p level.

Therefore, abstraction or substitution of the Cl ligand cannot be fully excluded.

The comparison of normal and grazing emission spectra in Fig. 3a reveals a decline of the Ru 3d_{5/2} signal at 80° by $\sim 50\%$ relative to the 0° signal, which indicates a depletion from the surface: a simple estimation, considering the inelastic mean free path of 2.8 nm for the Ru 3d photoelectrons and a thickness of the topmost IL layer of ~ 0.4 nm (height of an overall neutral layer of IL anions next to cations),⁴⁴ yields a signal reduction by 50%. Principally, a decrease at 80° could also be due to preferential orientation of the complex at the surface, with the tpy and/or bpy ligands (C_{aryl} atoms) pointing towards the vacuum, while the Ru–Cl entity is rather directed towards the bulk of the solution; however, for this situation, one expects a signal reduction by only $\sim 30\%$ at 80° in case of a perfect orientation. As we observe a significantly larger decrease, we propose a depletion of the complex from the topmost layer; nevertheless, some contributions due to orientational effects cannot be ruled out. For the N_{tpy/bpy} signal at 399.9 eV, a slight decrease is observed at 80°. Please note that the evaluation of the peak intensities of the N_{tpy/bpy} signal has a relatively large uncertainty due to the low concentration of the complex and the low cross-section of N 1s photoelectrons. The N_{Im} and F 1s signals show a weak decrease at 80°, while for the C_{alkyl/aryl} peak a clear enhancement was observed. This behavior is well-known for 1,3-alkylimidazolium-based ILs, where the cation shows a preferred orientation at the surface with the aliphatic side chains being directed towards the vacuum, as outlined above.^{4,5,38,45} The slightly larger increase of the C_{alkyl/aryl} signal than typically found for the C_{alkyl} signal of neat [C₄C₁Im][PF₆] (see Fig. S1, Table 1a and ref. 38, ESI†) is within the experimental uncertainty of our XPS measurements.

Nominal 2.5%_{mol} solution of [Ru(tpy)(dcb)Cl][PF₆] in [C₄C₁Im][PF₆]

As already discussed above, the solubility of [Ru(tpy)(bpy)Cl][PF₆] in [C₄C₁Im][PF₆] is relatively low. This situation worsens

when adding two carboxylic acid functional groups to the bipyridine ligand (see Fig. 1, $[\text{Ru}(\text{tpy})(\text{dcb})\text{Cl}][\text{PF}_6]$) yielding a suspension with an essentially undissolved complex, as concluded from visual inspection. Indeed, XPS spectra of a nominal 2.5%_{mol} solution of $[\text{Ru}(\text{tpy})(\text{dcb})\text{Cl}][\text{PF}_6]$ in $[\text{C}_4\text{C}_1\text{Im}][\text{PF}_6]$ (not shown) do not show any complex-related signals, *i.e.* adding two carboxylic acid functional groups to the bipyridyl ligand decreases the solubility of the complex in $[\text{C}_4\text{C}_1\text{Im}][\text{PF}_6]$ to an extent that the complex cannot be observed with XPS. When carboxylic acid functional groups are present in the complex, H-bonded structures are expected in the solid,⁴⁶ which may stabilize the crystal structure decreasing its solubility in $[\text{C}_4\text{C}_1\text{Im}][\text{PF}_6]$.

Nominal 2.5%_{mol} solution of $[\text{Ru}(\text{tpy})(\text{bpy})\text{Cl}][\text{PF}_6]$ in $[\text{C}_2\text{C}_1\text{Im}][\text{OAc}]$

Fig. 4a shows the C 1s/Ru 3d, N 1s, F 1s and O 1s XP spectra of a nominal 2.5%_{mol} solution of $[\text{Ru}(\text{tpy})(\text{bpy})\text{Cl}][\text{PF}_6]$ in $[\text{C}_2\text{C}_1\text{Im}][\text{OAc}]$ in normal and grazing emission (the full set of spectra along with a wide scan is depicted in Fig. S5 in the ESI†). While, as expected, the main peaks observed are due to solvent IL $[\text{C}_2\text{C}_1\text{Im}][\text{OAc}]$ (*cf.* Fig. 2), the Ru 3d_{5/2}, N_{tpy/bpy} and F 1s signals confirm the presence of the complex. In addition, Cl 2p and P 2p signals were detected with a very low intensity (see Fig. S5, ESI†). Fig. 4b depicts a more detailed view on the Ru 3d_{5/2} signal, revealing a major peak at 280.9 eV and a low-binding energy shoulder at 280.0 eV. Most notably, the major Ru 3d_{5/2} peak is at a similar position as in the equivalent $[\text{C}_4\text{C}_1\text{Im}][\text{PF}_6]$ solution (see Fig. 3) suggesting the same oxidation state and chemical environment of the metal center. The quantitative analysis of the peak intensities is shown in Table 1d and reveals that the total Ru 3d area at 0° agrees well with the nominal metal content. This finding is in line with the

visual inspection of a clear solution without any visual solid residuals with all of the Ru-complex being dissolved, which is in contrast to the $[\text{C}_4\text{C}_1\text{Im}][\text{PF}_6]$ solution. In 0° emission, the proportion of the low-binding energy species is roughly 1/5 of the total Ru 3d area.

More detailed information on the nature of this species can be obtained from the N 1s spectra, which overall are quite similar to the spectra described above. However, the quantitative analysis of the N_{tpy/bpy} signals in 0° emission reveals a significant stoichiometric deficiency of the ligands (by a factor of ~2). This could be due to substitution of about half of the polypyridyl ligands, which then evaporate under UHV conditions. Possible substitution agents could be the $[\text{OAc}]^-$ anion or NHCs present/forming in the solution alongside acetic acid. Similar to what has been observed for neat $[\text{C}_2\text{C}_1\text{Im}][\text{OAc}]$ (see above), acetic acid vapor was also detected for the solution of the complex by mass spectrometry as depicted in Fig. S3b in the ESI,† which indicates the presence of NHCs in solution. However, no direct XPS-evidence could be extracted from our spectra for coordination of NHCs to the metal center. For this, an additional peak shifted about ~1 eV³⁶ to lower binding energies relative to the N_{Im} signal is expected, which would overlay with both the N_{Im} and the N_{tpy/bpy} signal. For coordination of the $[\text{OAc}]^-$ anion to the metal center, a new species shifted to higher binding energy relative to the O 1s signal should be visible. In fact, the weak broad peak in the O 1s spectrum between at 532 and 534 eV is slightly more pronounced than found for neat $[\text{C}_2\text{C}_1\text{Im}][\text{OAc}]$, which would be in line with both coordination of NHCs (due to more pronounced formation of acetic acid) and $[\text{OAc}]^-$ (due to electron donation of the O atoms to the metal). Furthermore, the low binding energy component in the Ru 3d_{5/2} signal is compatible with an electron-donating ligand. Finally, it is worth noting that

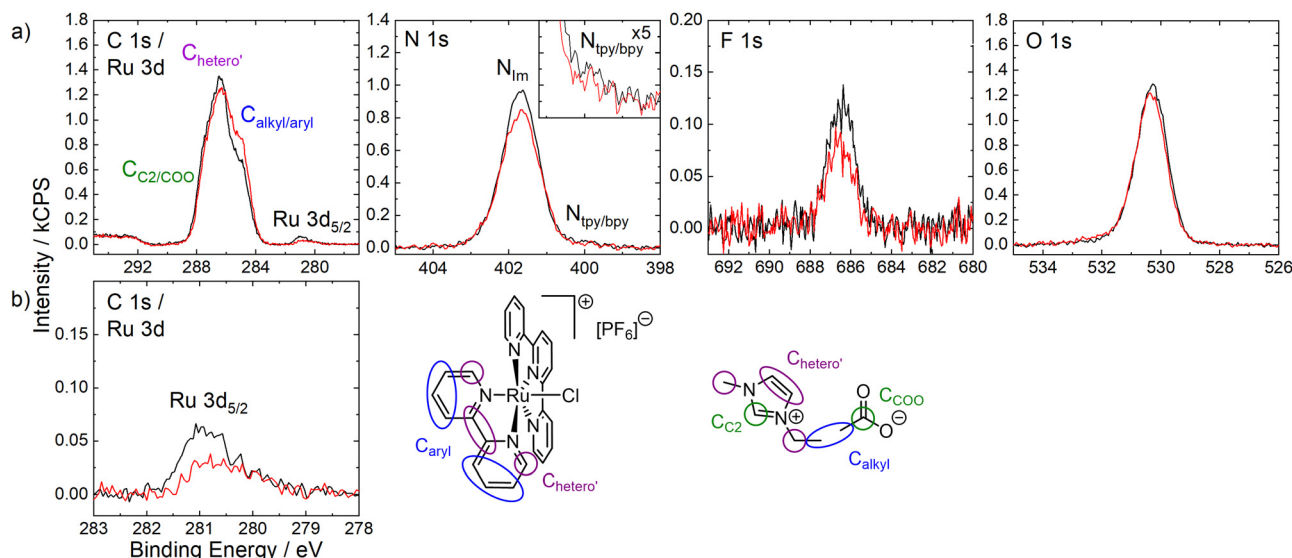


Fig. 4 (a) C 1s/Ru 3d (left), N 1s (middle left), F 1s (middle right) and O 1s (right) spectra of a nominal 2.5%_{mol} solution of $[\text{Ru}(\text{tpy})(\text{bpy})\text{Cl}][\text{PF}_6]$ in $[\text{C}_2\text{C}_1\text{Im}][\text{OAc}]$ in 0° (black) and 80° (red) emission with applied deconvolution and assignment of peaks to the molecular structure (note that for sake of clarity the assignment of carbon species from the ligands is only shown for bpy) and (b) more detailed view on Ru 3d region. All spectra were recorded at room temperature.

no changes of the spectra were observed over the typical measurement time for the whole set of spectra, which is shown in Fig. S6 (ESI[†]), ruling out pronounced beam damage effect being responsible for the low-binding energy Ru signal.

The 80° emission spectra reveal a pronounced decrease of the dominating high-binding energy Ru 3d_{5/2} signal to roughly half of the intensity detected at 0°, similar to the findings discussed for the [C₄C₁Im][PF₆] solution (see Fig. 4b and Table 1d); this behavior again indicates a depletion of the corresponding complex from the topmost layer. Interestingly, the low-binding energy Ru 3d_{5/2} peak shows similar intensity at 0° and 80°, indicating that this species is not surface-depleted but rather homogeneously distributed at the surface and in the bulk. We attribute this to a higher surface affinity of the species with the low Ru 3d_{5/2} binding energy. The F 1s signal of the complex counterions at 80° decreases to a smaller extent than the overall Ru signal, indicating that the counterion is depleted from the surface to a lower extent than the complex. Furthermore, the C_{alkyl/aryl} signal shows a significant increase at 80°, which is attributed due a preferential orientation of the [C₂C₁Im]⁺ and [OAc]⁻ ions of the solvent IL with the alkyl atoms pointing towards the vacuum side.

Nominal 2.5%_{mol} solution of [Ru(tpy)(dcb)Cl][PF₆] in [C₂C₁Im][OAc]

After preparation, the 2.5%_{mol} solution of [Ru(tpy)(dcb)Cl][PF₆] in [C₂C₁Im][OAc] solution showed the presence of a contamination, which was observed by a particularly intense C_{alkyl} at 285.0 eV and O 1s signal at 531.9 eV showing enhancement at 80°, probably due to a surface-active organic species. These species were successfully removed by mild sputtering the liquid sample with low energy Ar⁺ as done in the past for similar surface contaminations⁴⁷ (for details see Experimental section);

Fig. S7 in the ESI[†] contrasts the C 1s/Ru 3d and O 1s spectra obtained before and directly after sputtering. The Ru 3d_{5/2} signal was found at 280.9 eV without significant change in binding energy after the surface-cleaning procedure. This binding energy is also in accordance with the solutions discussed above, indicating intactness of the complex after treating the surface with sputtering.

The C 1s/Ru 3d, N 1s, F 1s and O 1s spectra of the solution after sputtering are shown in Fig. 5 (full set of spectra along with a wide scan is shown in Fig. S8, ESI[†]). The main signals stem from the IL, and the presence of the Ru(II) complex in solution is confirmed by the Ru 3d_{5/2} peak at 280.9 eV and the N_{tpy/dcb} signal at 399.9 eV. Table 1e shows the corresponding quantitative analysis of the ARXPS spectra: the Ru content, as deduced from the bulk-sensitive 0° spectra, is about half of the nominal metal concentration, which is in contrast to the solution of [Ru(tpy)(bpy)Cl][PF₆] in [C₂C₁Im][OAc]. This observation indicates that the presence of carboxylic acid functional groups decreases the solubility of the Ru complex, as is also evident from a minor amount of visible particles remaining undissolved. The Cl 2p XPS signals at 0° emission showed an intensity consistent with the 1:1 expected ratio with the Ru 3d_{5/2} XPS intensity. Furthermore, the N_{tpy/dcb} signal is consistent with the detected Ru signal, which is in contrast to the behavior of the solution of [Ru(tpy)(bpy)Cl][PF₆] in [C₂C₁Im][OAc], where a deficit of the N_{tpy/bpy} signal relative to the Ru signal was found, probably due to ligand substitution. This finding indicates the intactness of the [Ru(tpy)(dcb)Cl]⁺ cation in [C₂C₁Im][OAc], which could be due to the presence of the carboxylic acid/carboxylate functional groups in the ligands potentially resulting in a more inert complex.⁴⁸ By comparing the normal and grazing emission spectra, similar effects as discussed above become evident. The Ru 3d_{5/2} peak and the

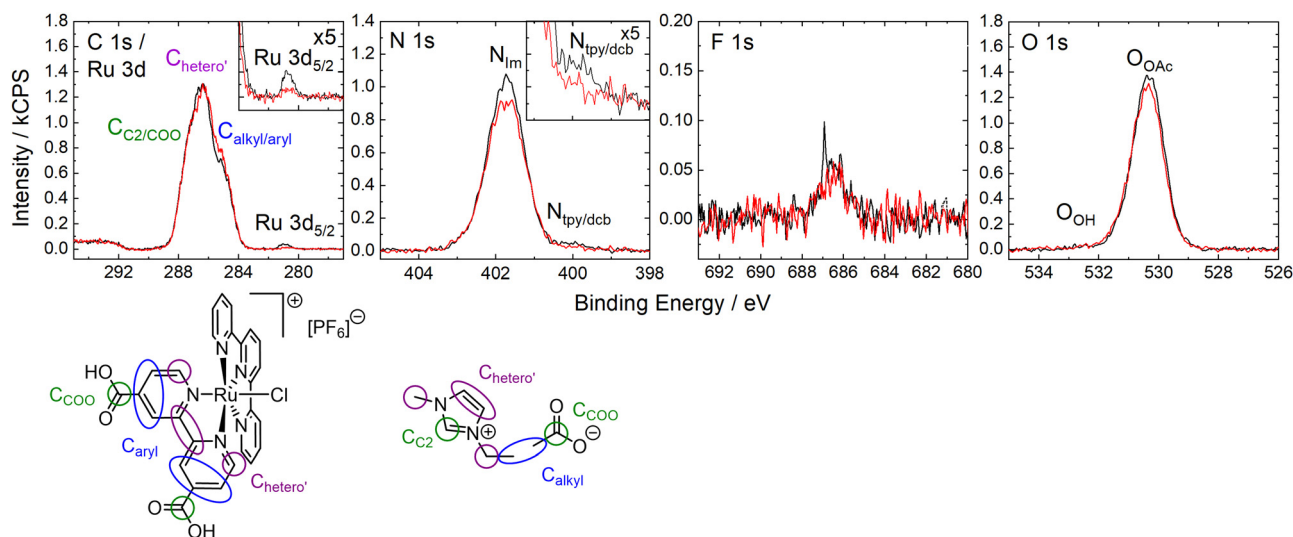


Fig. 5 C 1s/Ru 3d (left), N 1s (middle left), F 1s (middle right) and O 1s (right) spectra of a nominal 2.5%_{mol} solution of [Ru(tpy)(dcb)Cl][PF₆] in [C₂C₁Im][OAc] in 0° (black) and 80° (red) emission with applied deconvolution and assignment of peaks to the molecular structure (note that for sake of clarity the assignment of carbon species from the ligands is only shown for dcb). The surface of the sample was cleaned by sputtering prior to the measurement. All spectra were recorded at room temperature.

$N_{\text{bpy}/\text{dcb}}$ show a significant decrease at 80° . Overall, the complex shows a similar behavior as the derivatives discussed above and is depleted from the topmost surface layer.

Conclusions

We conducted ARXPS measurements on solutions of $[\text{Ru}(\text{tpy})(\text{bpy})\text{Cl}][\text{PF}_6]$ and $[\text{Ru}(\text{tpy})(\text{dcb})\text{Cl}][\text{PF}_6]$ in $[\text{C}_4\text{C}_1\text{Im}][\text{PF}_6]$ and $[\text{C}_2\text{C}_1\text{Im}][\text{OAc}]$, all with the same nominal concentration of 2.5%_{mol}. In $[\text{C}_4\text{C}_1\text{Im}][\text{PF}_6]$, the chemical environment of the metal center in $[\text{Ru}(\text{tpy})(\text{bpy})\text{Cl}][\text{PF}_6]$ remains preserved. However, when dissolved in $[\text{C}_2\text{C}_1\text{Im}][\text{OAc}]$, the metal center in $[\text{Ru}(\text{tpy})(\text{bpy})\text{Cl}][\text{PF}_6]$ undergoes partial changes in the chemical environment, probably by ligand exchange. The presence of carboxylic acid functional groups in the bipyridyl ligand in $[\text{Ru}(\text{tpy})(\text{dcb})\text{Cl}][\text{PF}_6]$ seems to inhibit ligand exchange. For all solutions but $[\text{Ru}(\text{tpy})(\text{bpy})\text{Cl}][\text{PF}_6]$ in $[\text{C}_2\text{C}_1\text{Im}][\text{OAc}]$, we found a lower Ru intensity than expected from the nominal weigh-in, which is accordance with a lower solubility of the respective complexes in the ILs. Overall, all complexes investigated herein do not exhibit segregation to the IL/gas interface. The XPS signals originating from the investigated Ru complexes rather show a clear decrease at grazing emission, suggesting that the metal is not directly present at the outer surface. This behavior is attributed to a depletion of the complex from the topmost layer. These findings provide a basis for targeted manipulation of the IL/gas interface, e.g. for SILP catalysis. We are currently investigating rational modification of the ligand system for surface segregation of these catalysts.

Conflicts of interest

There are no conflicts to declare.

Acknowledgements

Luciano Sanchez Merlinsky acknowledges a PhD scholarship from CONICET. Financial support from Agencia I + D + i (PICT 2018-03276), Universidad de Buenos Aires (UBACyT 2020) and CONICET (PIP 2021) is gratefully acknowledged. Federico Williams thanks DAAD for financial funding. Daniel Hemmeyer, Florian Maier and Hans-Peter Steinrück acknowledge the Deutsche Forschungsgemeinschaft (DFG, German Research Foundation) for financial support (Project-ID 431791331 – SFB 1452). Daniel Hemmeyer furthermore thanks the Stiftung Stipendien-Fonds of the German chemical industry association (Verband der Chemischen Industrie, VCI) for a Kekulé fellowship.

References

- 1 A. Riisager, R. Fehrmann, M. Haumann and P. Wasserscheid, *Eur. J. Inorg. Chem.*, 2006, 695–706.
- 2 A. Riisager, R. Fehrmann, S. Flicker, R. van Hal, M. Haumann and P. Wasserscheid, *Angew. Chem., Int. Ed.*, 2005, **44**, 815–819.
- 3 J. Scholz, V. Hager, X. Wang, F. T. U. Kohler, M. Sternberg, M. Haumann, N. Szesni, K. Meyer and P. Wasserscheid, *ChemCatChem*, 2014, **6**, 162–169.
- 4 H.-P. Steinrück and P. Wasserscheid, *Catal. Lett.*, 2015, **145**, 380–397.
- 5 H.-P. Steinrück, J. Libuda, P. Wasserscheid, T. Cremer, C. Kolbeck, M. Laurin, F. Maier, M. Sobota, P. S. Schulz and M. Stark, *Adv. Mater.*, 2011, **23**, 2571–2587.
- 6 C. Kolbeck, N. Paape, T. Cremer, P. S. Schulz, F. Maier, H.-P. Steinrück and P. Wasserscheid, *Chem. – Eur. J.*, 2010, **16**, 12083–12087.
- 7 E. J. Smoll, Jr., X. Chen, L. M. Hall, L. D'Andrea, J. M. Slattery and T. K. Minton, *J. Phys. Chem. C*, 2020, **124**, 382–397.
- 8 F. Maier, J. M. Gottfried, J. Rossa, D. Gerhard, P. S. Schulz, W. Schwieger, P. Wasserscheid and H.-P. Steinrück, *Angew. Chem., Int. Ed.*, 2006, **45**, 7778–7780.
- 9 C. Kolbeck, N. Taccardi, N. Paape, P. S. Schulz, P. Wasserscheid, H.-P. Steinrück and F. Maier, *J. Mol. Liq.*, 2014, **192**, 103–113.
- 10 D. Hemmeyer, D. Kremitzl, P. S. Schulz, P. Wasserscheid, F. Maier and H.-P. Steinrück, *Chem. – Eur. J.*, 2023, **29**, e202203325.
- 11 D. Hemmeyer, U. Paap, F. Maier and H.-P. Steinrück, *Catalysts*, 2023, **13**, 871.
- 12 D. Hemmeyer, U. Paap, N. Taccardi, J. Mehler, P. S. Schulz, P. Wasserscheid, F. Maier and H.-P. Steinrück, *ChemPhysChem*, 2023, **24**, e202200391.
- 13 D. Hemmeyer, U. Paap, N. Wellnhofer, A. Gezmis, D. Kremitzl, P. Wasserscheid, H.-P. Steinrück and F. Maier, *ChemPhysChem*, 2023, **24**, e202300612.
- 14 S. Men, K. R. J. Lovelock and P. Licence, *RSC Adv.*, 2015, **5**, 35958–35965.
- 15 T. Welton, *Coord. Chem. Rev.*, 2004, **248**, 2459–2477.
- 16 J. D. Knoll and C. Turro, *Coord. Chem. Rev.*, 2015, **282–283**, 110–126.
- 17 V. Balzani, G. Bergamini and P. Ceroni, *Coord. Chem. Rev.*, 2008, **252**, 2456–2469.
- 18 M. Grätzel, *Acc. Chem. Res.*, 2009, **42**, 1788–1798.
- 19 D. L. Ashford, M. K. Gish, A. K. Vannucci, M. K. Brennaman, J. L. Templeton, J. M. Papanikolas and T. J. Meyer, *Chem. Rev.*, 2015, **115**, 13006–13049.
- 20 S. E. Domínguez, M. V. Juárez, G. E. Pieslinger and L. M. Baraldo, *Eur. J. Inorg. Chem.*, 2022, e202100843.
- 21 R. C. Buijsman, E. van Vuuren and J. G. Sterrenburg, *Org. Lett.*, 2001, **3**, 3785–3787.
- 22 D. Sémeril, H. Olivier-Bourbigou, C. Bruneau and P. H. Dixneuf, *Chem. Commun.*, 2002, 146–147.
- 23 N. Audic, H. Clavier, M. Mauduit and J.-C. Guillemin, *J. Am. Chem. Soc.*, 2003, **125**, 9248–9249.
- 24 Q. Yao and Y. Zhang, *Angew. Chem., Int. Ed.*, 2003, **42**, 3395–3398.
- 25 C. Cesari, A. Cingolani, M. Teti, A. Messori, S. Zacchini, V. Zanotti and R. Mazzoni, *Eur. J. Inorg. Chem.*, 2020, 1114–1122.
- 26 S.-P. Xia, G.-R. Ding, R. Zhang, L.-J. Han, B.-H. Xu and S.-J. Zhang, *Green Chem.*, 2021, **23**, 3073–3080.

- 27 I. Niedermaier, C. Kolbeck, H.-P. Steinrück and F. Maier, *Rev. Sci. Instrum.*, 2016, **87**, 045105.
- 28 B. P. Sullivan, J. M. Calvert and T. J. Meyer, *Inorg. Chem.*, 1980, **19**, 1404–1407.
- 29 K.-Y. Liu, C.-L. Hsu, S.-H. Chang, J.-G. Chen, K.-C. Ho and K.-F. Lin, *J. Polym. Sci., Part A: Polym. Chem.*, 2010, **48**, 366–372.
- 30 K. J. Takeuchi, M. S. Thompson, D. W. Pipes and T. J. Meyer, *Inorg. Chem.*, 1984, **23**, 1845–1851.
- 31 C. D. Wagner, L. E. Davis, M. V. Zeller, J. A. Taylor, R. H. Raymond and L. H. Gale, *Surf. Interface Anal.*, 1981, **3**, 211–225.
- 32 I. Chiarotto, L. Mattiello, F. Pandolfi, D. Rocco and M. Feroci, *Front. Chem.*, 2018, **6**, 355.
- 33 I. Chiarotto, M. Feroci, G. Forte, M. Orsini and A. Inesi, *ChemElectroChem*, 2014, **1**, 1525–1530.
- 34 O. Hollóczki, D. Gerhard, K. Massone, L. Szarvas, B. Németh, T. Veszprémi and L. Nyulászi, *New J. Chem.*, 2010, **34**, 3004–3009.
- 35 L. Álvarez-Rodríguez, J. A. Cabeza, P. García-Álvarez and E. Pérez-Carreño, *Organometallics*, 2018, **37**, 3399–3406.
- 36 S. Men and J. Jiang, *Russ. J. Phys. Chem. A*, 2018, **92**, 1627–1630.
- 37 Y. Zhang, Y. Khalifa, E. J. Maginn and J. T. Newberg, *J. Phys. Chem. C*, 2018, **122**, 27392–27401.
- 38 B. S. J. Heller, M. Lexow, F. Greco, S. Shin, G. Partl, F. Maier and H.-P. Steinrück, *Chem. – Eur. J.*, 2020, **26**, 1117–1126.
- 39 P. Aydogan Gokturk, U. Salzner, L. Nyulászi, B. Ulgut, C. Kocabas and S. Suzer, *Electrochim. Acta*, 2017, **234**, 37–42.
- 40 NIST Mass Spectrometry Data Center, W. E. Wallace, director, in *NIST Chemistry WebBook*, NIST Standard Reference Database Number 69, ed. P. J. Linstrom and W. G. Mallard, National Institute of Standards and Technology, Gaithersburg MD, 20899, (retrieved April 13, 2022), ch. Mass Spectra, 2023.
- 41 R. E. Shepherd, A. Proctor, W. W. Henderson and T. K. Myser, *Inorg. Chem.*, 1987, **26**, 2440–2444.
- 42 S. Men and J. Jiang, *Chem. Phys. Lett.*, 2016, **646**, 125–129.
- 43 S. Men and Y. Jin, *Russ. J. Phys. Chem. A*, 2018, **92**, 2472.
- 44 M. Lexow, F. Maier and H.-P. Steinrück, *Adv. Phys.: X*, 2020, **5**, 1761266.
- 45 H.-P. Steinrück, *Phys. Chem. Chem. Phys.*, 2012, **14**, 5010–5029.
- 46 A. Nielsen, C. J. McKenzie and A. D. Bond, *Acta Crystallogr., Sect. E: Struct. Rep. Online*, 2012, **68**, m77–78.
- 47 C. Kolbeck, M. Killian, F. Maier, N. Paape, P. Wasserscheid and H.-P. Steinrück, *Langmuir*, 2008, **24**, 9500–9507.
- 48 A. B. P. Lever, *Inorg. Chem.*, 1990, **29**, 1271–1285.